

Method for Designing and Testing an Ultrasonic Range Finder

JeanReno C. Racines, Maxwell W. Sotnick

Department of Electrical Engineering

California Polytechnic State University, San Luis Obispo

San Luis Obispo, CA, USA

jracines@calpoly.edu, msotnick@calpoly.edu

Abstract—This paper presents a method to build and test a short-distance ultrasonic range finder. The approach involves using a microcontroller to transmit and detect a 40kHz pulse along with measure distance from the pulse's time of flight. This study explains the device's design and derives each sub module's operation.

Keywords—Ultrasonic Transducer, Bandwidth, Amplifier, Distance measurement, Path-Loss, Time of flight, One-Shot, Phase-locked loop, Oscillator

I. INTRODUCTION

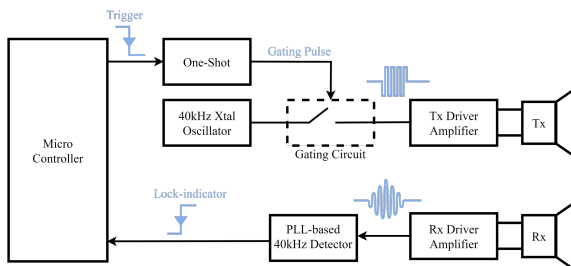


Fig. 1. The high-level block diagram of the range finder. Dr. Prodonov offers this design suggestion in the laboratory manual for the Cal Poly course EE449 [1].

Fig. 1 above presents a high-level representation of the range finder featuring its key modules. This paper covers these modules in-depth, explaining how to design and test them. The design employs an ultrasonic transducer pair whose center frequency is 40kHz [2]. The microcontroller, an Arduino Nano, triggers a 40khz burst out of the transmitter and then detects its reflection via the receiver after it hits an object such as a wall. The duration between the trigger pulse and the reflected signal detection is the time of flight, which helps detect the distance between the range finder and the object. For the course, a breadboard sufficed for this circuit. Since the instructor remotely delivered this course, the Analog Discovery 2 (AD2) served as the oscilloscope, power supply, waveform generator, and network analyzer. The AD2, a USB-powered device, outputs between -5V to 5V.

II. ULTRASONIC TRANSDUCERS

A. Ultrasonic Transducer: Theory

The 40TR12B-R ultrasonic transmitter and receiver pair used in this device has a center frequency of 40kHz, above the

frequency range of human hearing [2]. While the device requires a line of sight with the target to successfully transmit and receive, the known sound propagation speed in the air makes it simple to calculate distance. Since the 40TR12B-R's center frequency is 40kHz, it only passes signals around that frequency. Thus, even though a square wave, a signal composed of infinitely many harmonics, is the input, the transmitter only passes the 40kHz component. It shows bandpass behavior that the paper explores in later sections.

The transducer pair converts electrical energy into ultrasound energy and back. The AC voltage inputted into the transmitter transducer causes a piezoelectric resonator to oscillate at the 40kHz center frequency. This signal propagates through the air at the speed of the sound, reflects off an object, and causes the receiver's piezoelectric crystal to vibrate, which the transducer then converts back into electrical energy.

B. Ultrasonic Transducer: Design and Experimentation

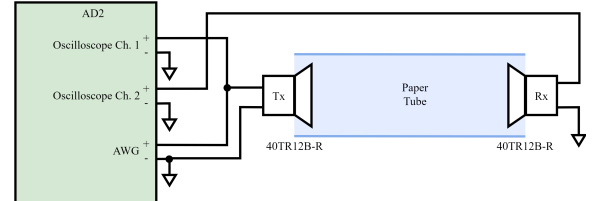


Fig. 2. The experimental circuit that obtained the frequency and transient response of the 40TR12B-R ultrasonic pair.

The first stage of the design involved testing the transducer pair without any amplifiers on either side to verify its center frequency of 40kHz and its bandpass behavior. The diagram shown in Fig. 2 depicts the experimental setup. The AD2 drove the transmitter (Tx) transducer and produced an ultrasonic signal that the receiver (Rx) transducer detected and converted back into an electrical signal. The AD2 also measured both sides using its oscilloscope. To prevent erroneous interference, the pair pointed towards each other inside a paper tube.

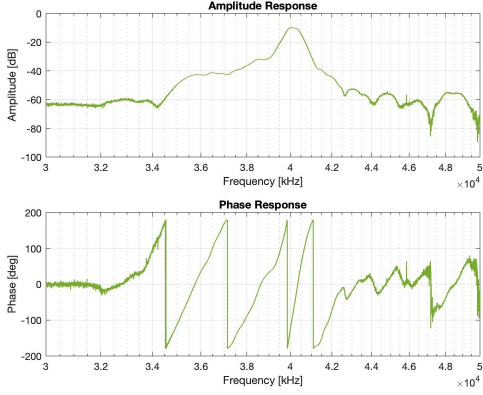


Fig. 3. The top graph depicts the magnitude (dB) frequency response of the transducer pair with oscilloscope Ch. 1 on the transmitter side and Ch. 2 on the receiver side. The bottom graph represents the phase frequency response. Matlab plotted the AD2 data.

The plot in Fig. 3 shows the frequency and phase response of the transducer pair. The center frequency was at 40kHz since the magnitude attenuation reached a minimum there at around -10dB. Elsewhere, it was below -60dB.

It was also desirable to observe the transducers' step response which Fig. 4 shows below. The arbitrary waveform generator (AWG) sent a -4.5 to 4.5 1Hz step response into the Tx transducer and the response on the Rx side was a single 40kHz wavelet lasting for around 2.5ms. While the input is on a 1V/div scale, the wavelet was on a 20mV/div scale. The received signal amplitude was many orders smaller than that of the input amplitude.

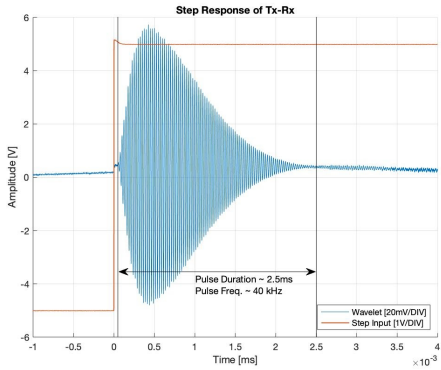


Fig. 4. The transducers' response (blue) to a step input (orange). Matlab plotted the AD2 data.

C. Ultrasonic Transducer: Bandpass Behavior

The Tx and Rx transducers each exhibit a 2nd order bandpass behavior. Therefore, the pair collectively exhibits a 4th order bandpass behavior. Given the data collected of the 4th order bandpass behavior, it is possible to determine the individual quality factors and center frequencies of the two 2nd order bandpasses. From the amplitude dataset, it is also possible to utilize a tool, such as MATLAB's System ID Toolbox, to estimate the 4th order transfer function given by the Tx-Rx pair.

$$H(s) = \frac{(5.9148 \times 10^{10})s^2 + (1.5775 \times 10^{13})s + (7.4176 \times 10^{19})}{s^4 + (2.75 \times 10^3)s^3 - (4.64 \times 10^9)s^2 + (5.06 \times 10^{12})s - (4.0381 \times 10^{18})}$$

Using the expression above, the same MATLAB library gave these metrics:

$$\begin{aligned} \omega_0 &= 39.98 \text{ kHz} & \omega_0 &= 40.28 \text{ kHz} \\ \omega_{c1} &= 39.75 \text{ kHz} & \omega_{c1} &= 40.04 \text{ kHz} \\ \omega_{c2} &= 40.21 \text{ kHz} & \omega_{c2} &= 40.5 \text{ kHz} \\ BW &= 460 \text{ Hz} & BW &= 500 \text{ Hz} \\ Q &\approx 86.9 & Q &\approx 80.56 \end{aligned}$$

III. TRANSMITTER DRIVER AMPLIFIER

A. Transmitter Driver Amplifier: Theory

To ensure robust transmission, a steady input voltage into the Tx transducer is desirable. The TC4428AEPA current driver served to overcome this issue. This is a MOSFET gate driver capable of output currents up to 1.5A, more than enough for the application [3]. Also according to its datasheet, the logic '1' input voltage is 2.4V and the logic '0' voltage is anywhere below 0.8V [3].

B. Transmitter Driver Amplifier: Design and Experimentation

The circuit in Fig. 5 presents the experimental setup: the TC4428AEPA drove the Tx transducer. Ch.1 of the AD2 oscilloscope measured the input to the Tx driver while Ch.2 measured the output of the Rx transducer. The AD2 also supplied the power rails of the TC4428AEPA and bypass capacitors eliminated any noise on those power rails as well as any driver-induced interference.

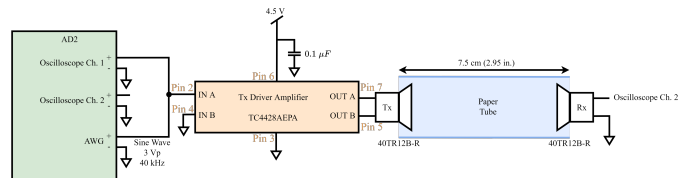


Fig. 5. The experimental circuit used to test the TC4428AEPA Tx driver amplifier. The diagram also shows the pins of the driver IC in orange.

To test this, the AWG from the AD2 supplied a 3V_p 40kHz sine wave into the input of the Tx driver. Again, the paper tube served to eliminate any extraneous noise that may have disrupted the results. Oscilloscope Ch.1 measured that input while Ch.2 measured the output of the Rx transducer which had a magnitude of around 1.41V_p. The image in Fig. 6 below shows a scope capture from the AD2.

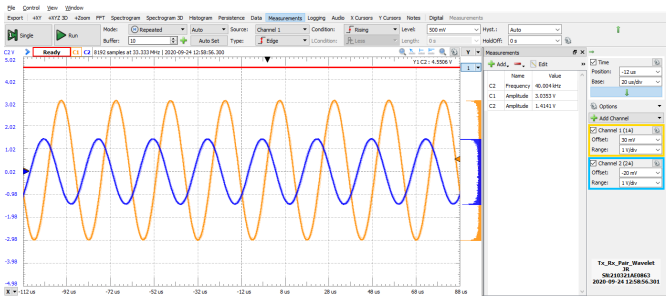


Fig. 6. The figure above shows the AWG input into the Tx driver on oscilloscope Ch.1 (orange) while Ch.2 shows the output of the Rx transducer. The time base is 20 μ s and the voltage base is 1V/div.

IV. RECEIVER AMPLIFIER

A. Receiver Amplifier: Theory

As shown previously in Fig. 4, the transducers' response to a step input showed that the received signal on the Rx transducer had an amplitude in the sub 100mV range. This was far too small for the tone decoder to detect this signal, so an amplifier was necessary to boost this signal to an acceptable amplitude. An LM358P-based non-inverting amplifier was a suitable solution [4]. Fig. 7 below shows a general non-inverting operational amplifier (op-amp) configuration. The pulldown resistor R_3 put a well-defined voltage at the non-inverting terminal of the amplifier. The 0.1 μ F bypass capacitors reduced any noise on the power supply. The transfer function was easily obtained, with $s = j\omega = j(2\pi)f$, via the assumption of an ideal op-amp. The magnitude of that equation yielded the gain of the amplifier in V/V.

$$v^+ = v^-$$

$$v^- = V_i = V_o \frac{R_1 + \frac{1}{sC}}{R_2 + R_1 + \frac{1}{sC}}$$

$$H(s) = \frac{V_o}{V_i} = \frac{R_2}{R_1 + \frac{1}{sC}} + 1 \quad (1)$$

$$20 \log_{10} |H(s)| = dB$$

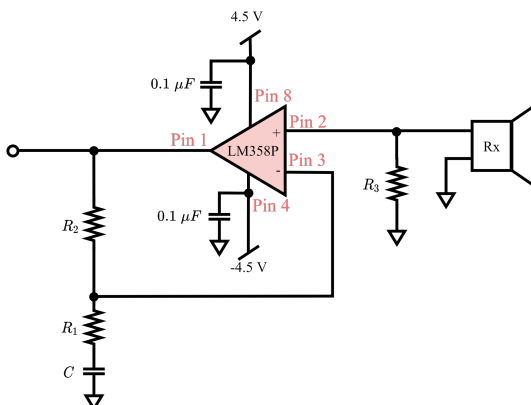


Fig. 7. The figure above shows a non-inverting op-amp used in the Rx amplifier.

B. Receiver Amplifier: Design and Experimentation

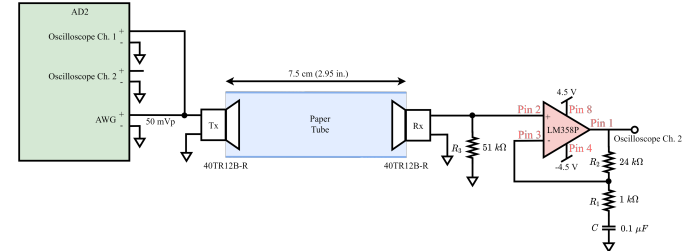


Fig. 8. The circuit used to test the Rx amplifier. Again, the AD2 supplied the +/-4.5 voltage rails. The diagram also shows the pins of the LM358P in red.

Fig. 8 above shows the experimental setup for the preliminary amplifier design. A single op-amp configuration sufficed. The target specification was 20dB (or 10V/V) gain at 40kHz. Using (1) with the chosen values of $R_1 = 1k\Omega$, $R_2 = 10k\Omega$, and $R_3 = 51k\Omega$ yields a gain of around 20.82dB (or 10.99 V/V) at 40kHz. This expected gain appeared in the frequency response of Fig. 9 below. Note that the unused op-amp must remain in a unity gain configuration to prevent any damage to the IC.

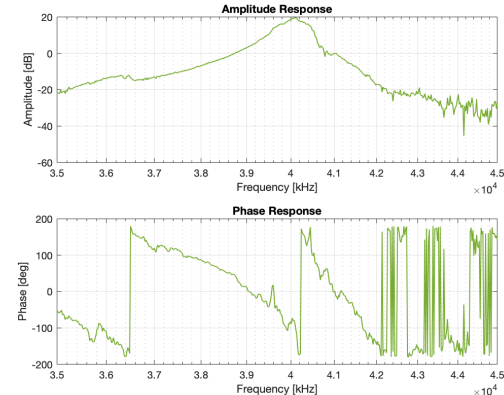


Fig. 9. The frequency response of the current transducer system using the preliminary Rx amplifier design. Matlab plotted the AD2 data.

C. Receiver Amplifier: Improvements

Improvements to the Rx amplifier began with creating a relationship between the path-loss of the amplifier and the distance from it and an object such as a wall. First, it is imperative to define the best- and worst-case scenarios of this transducer system. The worst-case is a single voltage step input into the transmitter side. As shown previously, this produced a low-amplitude wavelet. Conversely, the best case is multiple step inputs or a square wave. Each step, whether positive or negative, creates a wavelet on the Rx side. The multiple wavelets then superimpose on each other, creating a new wavelet of longer duration and whose amplitude is more defined. Fig. 10 below depicts this observation.

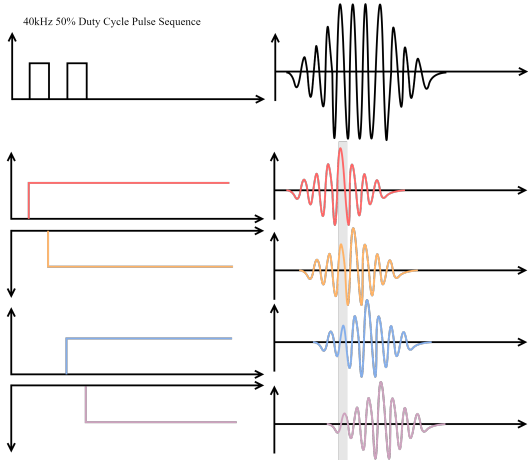


Fig. 10. The best- and worst-case inputs of the transducer system.

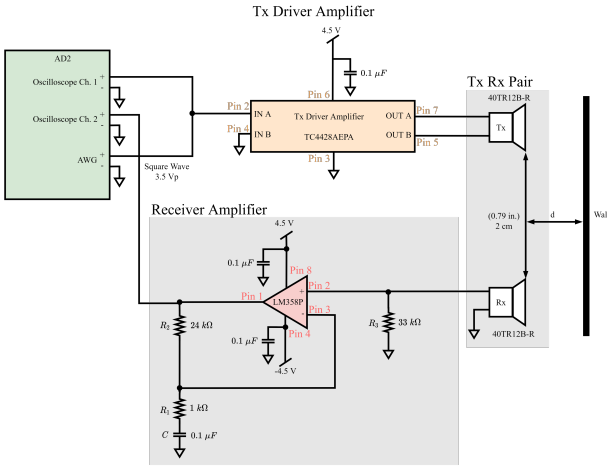


Fig. 11. The experimental circuit of the Tx-Rx system positioned to transmit a signal towards the wall.

The circuit in Fig. 11 shows the experimental setup to test the best and worst case of the amplifier. The input from the AWG into the Tx driver was a $3.5V_p$ square wave. The distance d was measured between the transducer and a wall. Measuring the signal received on the Rx transducer for various values of d determined a relationship between the path-loss and distance from the object. The AD2 measured the input into the Tx driver as well as the output of the Rx amplifier. The AD2 also supplied the voltage rails for both ICs. Table I shows the data obtained from these measurements. The voltage received in the worst-case scenario was at a minimum while the opposite is true for the best-case.

TABLE I. BEST- AND WORST-CASE ULTRASONIC TRANSMISSION USING PRELIMINARY RECEIVER AMPLIFIER CONFIGURATION

Distance (in.)	The output of the Receiver Amplifier	
	Best-Case Voltage (mV)	Worst-Case Voltage (mV)
1	62.414	1505.9
2	50.923	1344.8
4	29.335	1103.4
6	21.252	931.03
8	16.724	620.69
10	12.845	482.76
12	11.121	327.59
24	10.776	224.14
36	7.0730	158.62
48	6.4863	151.72
60	6.4863	168.97
72	7.2034	158.62
84	6.5515	151.72

From the path-loss versus distance data, the received signal required amplification since the tone decoder's smallest detectable input voltage is around $20mV_{rms}$ [5]. The circuit shown in Fig. 12 shows a new cascaded Rx amplifier. Using (2) and the chosen values of $R_1 = 10k\Omega$, $R_2 = 51k\Omega$, $R_3 = 33k\Omega$, $R_4 = 10k\Omega$, $R_5 = 51k\Omega$ yielded a gain of $30.823dB$ (or $34.765 V/V$). This amplifier showed a noticeable gain in the path-loss versus distance data points in Table II.

$$H_1(s) = \frac{R_2}{R_1 + \frac{1}{sC}} + 1, \quad H_2(s) = \frac{R_5}{R_4} + 1$$

$$H_{EQ}(s) = H_1(s)H_2(s)$$

$$H_{EQ}(s) = \left(\frac{R_2}{R_1 + \frac{1}{sC}} + 1 \right) \left(\frac{R_5}{R_4} + 1 \right) \quad (2)$$

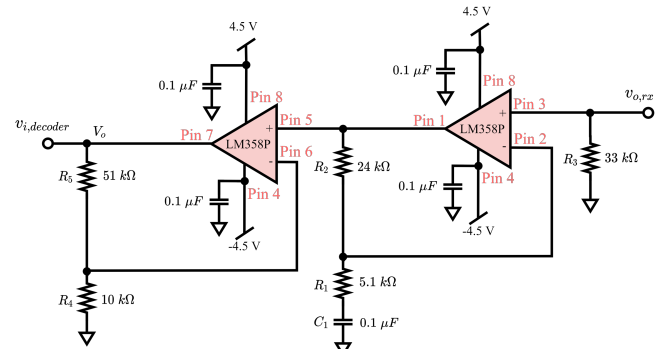


Fig. 12. The cascaded Rx amplifier shown ensured the tone decoder could detect the received signal.

TABLE II. BEST- AND WORST-CASE ULTRASONIC TRANSMISSION USING CASCDED RECEIVER AMPLIFIER CONFIGURATION

Distance (in.)	The output of the Receiver Amplifier	
	Best-Case Voltage (mV)	Worst-Case Voltage (mV)
1	146.66	1621.8
2	111.48	1608.7
4	68.266	1578.8
6	60.886	1552.6
8	47.970	1542.2
10	42.435	1494.5
12	35.055	1402.2
24	27.675	1014.8
36	28.598	901.61
48	26.753	922.51
60	25.830	867.16
72	26.753	904.06
84	24.908	885.61

V. ONE-SHOT AND GATING CIRCUIT

A. One-Shot: Theory

The one-shot module accurately controlled the duration of the pulse sent to the Tx driver. The monostable configuration of a 555 timer (ICM7555IPAZ) shown in Fig. 13a is a one-shot circuit that, when triggered, outputs a logic high with a controlled duration [6].

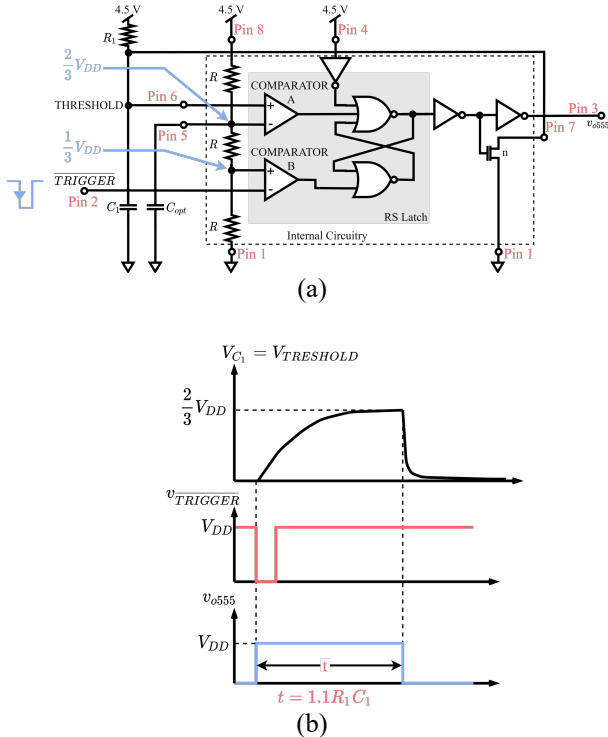


Fig. 13. (a) The internal and external circuitry of the monostable-connected ICM7555IPAZ timer. (b) Key voltages in the monostable timer.

Fig. 13b shows plots of key voltages in the monostable 555 timer operation. Note that the trigger input (pin 2) must be high before v₀₅₅₅ can return to a low state. Thus, the length of the trigger pulse must be around 3-10x smaller than the desired output pulse duration. (3) determines the duration t of v₀₅₅₅. For example, given R₁ = 25kΩ and C₁ = 47nF, (3) says that t ≈ 1.24ms.

$$\begin{aligned}
 V_{C_1} &= V_{DD}(1 - e^{-\frac{t}{R_1 C_1}}) \\
 \frac{2}{3} V_{DD} &= V_{DD}(1 - e^{-\frac{t}{R_1 C_1}}) \\
 e^{-\frac{t}{R_1 C_1}} &= \frac{1}{3} \Rightarrow \ln\left(e^{-\frac{t}{R_1 C_1}}\right) = \ln\left(\frac{1}{3}\right) \\
 t &= -R_1 C_1 \ln\left(\frac{1}{3}\right) = 1.1 R_1 C_1
 \end{aligned} \tag{3}$$

The output v₀₅₅₅ serves as the input to the non-inverting terminal of an LM393-based comparator gating circuit. Since the LM393 has an open collector output stage, its output pulled down to ground when the non-inverting terminal's voltage was lower than the inverting terminal [7]. Therefore, the 40kHz oscillator V₅ in the LTSpice simulation of Fig. 14a only passes through to the Tx driver when v₀₅₅₅ goes high. The CR-diode circuit composed of C₃, R₃, and D₃ ensures the trigger pulse is always much shorter than the desired output pulse of the 555 timer. This is the triggering network. D₂ protects the IC from positive input spikes that may exceed the chip's supply rails. The plots in Fig. 14b show the output of the triggering network, the duration of v₀₅₅₅ for R₁ = 25kΩ and C₁ = 47nF, and the 40kHz burst that lasts for that same duration out of the gating circuit.

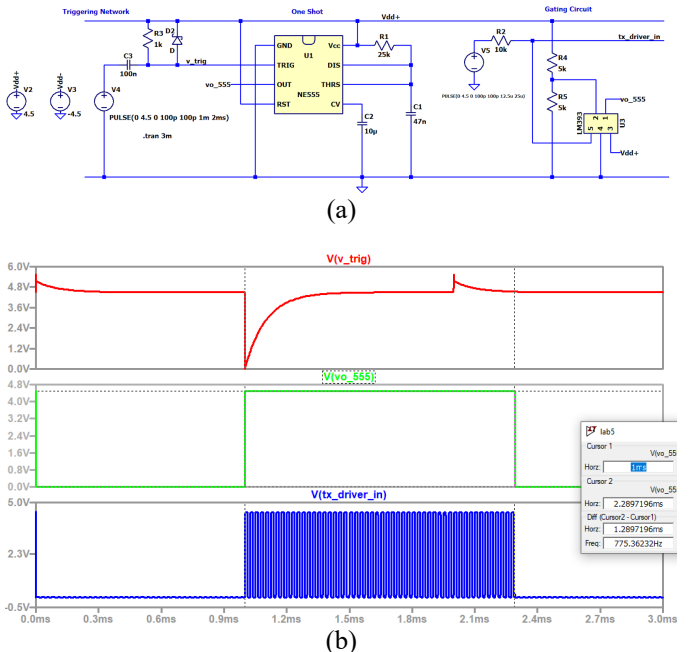


Fig. 14. (a) The LTSpice model circuit for the ICM7555IPAZ monostable configuration and the LM393-based comparator gating circuit. (b) The simulated triggering network output shown in red on top of the one-shot circuit

output shown in green for $R_1 = 25k\Omega$ and $C_1 = 47nF$. Shown in blue is the output of the gating circuit.

B. One-Shot: Design and Experimentation

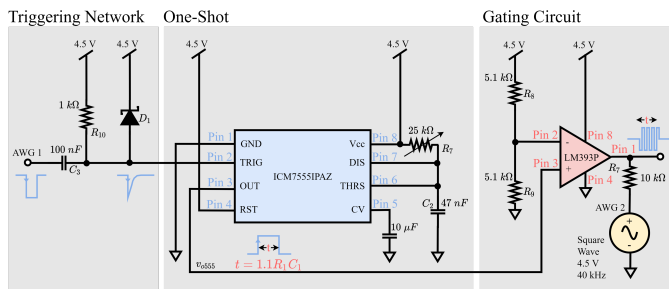


Fig. 15. The experimental setup to test the triggering network, one-shot, and gating circuit.

The circuit in Fig. 15 covers the experimental setup for testing the one-shot circuit. The AD2's first AWG supplied the triggering signal to the 555 timer while the second AWG supplied the 40kHz oscillator at the output of the gating circuit. In Fig. 16, the AD2's oscilloscope Ch.1 measured the output of the triggering network (pin 2 of the ICM7555IPAZ) while Ch.2 measured the output (pin 1 of the LM393) of the gating circuit. The output results of the experimental circuit coincided with the LTSpice simulation.

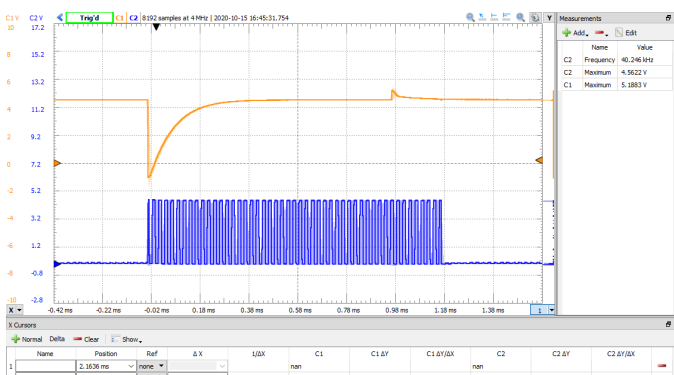


Fig. 16. An oscilloscope plot where Ch.1 (orange) measured the output of the triggering network and Ch.2 (blue) measured the output of the gating circuit. The length of the 40kHz burst was around 1.29ms.

VI. TONE DECODER

A. Tone-Decoder: Theory

The output of the Rx amplifier goes into the input of a tone decoder which detects the presence of a 40kHz frequency. The tone decoder uses a phase-locked loop (PLL), which has the general topology shown in Fig. 17.

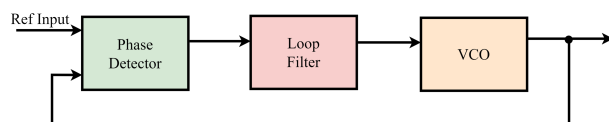


Fig. 17. Basic block diagram of a phase-locked loop.

The LM567CN is a general-purpose tone decoder chosen for its touch-tone decoding capabilities, only one out of its several

possible applications [5]. Fig. 18 shows the high-level block diagram for this IC configured as a tone decoder. Internally, it implements a PLL such that the user can fix the VCO to a certain frequency. It also features an I (in-phase) and Q (quadrature) phase detector, driven by the VCO [5]. Together, this system provides a switch to ground at its output (pin 8) when the input (pin 3) signal frequency matches the center frequency. The external timing resistor and capacitor set this center frequency.

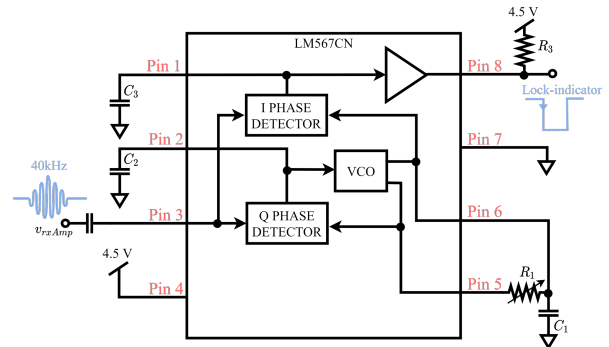


Fig. 18. The high-level block diagram of the LM567CN's internal subcircuits [5].

For the range finder, the center frequency of the tone detector must be 40kHz. This is the free-running frequency of the VCO so pin 6 and pin 7 should oscillate at that frequency as well. The LM567CN's datasheet provides (4) to set this frequency using the timing components R_1 and C_1 [5].

$$f_o \approx \frac{1.1}{R_1 C_1} \quad (4)$$

The datasheet also provides (5) to set the detection bandwidth (BW) with C_2 for input signals below 200mV. However, since the inputs signals can exceed 200mV, the datasheet has a lookup table to choose C_2 for a desired bandwidth [5]. Lastly, (6) determines the output filter capacitor C_3 .

$$BW = 1070 \sqrt{\frac{V_i}{f_o C_2}} \text{ in \% of } f_o \quad (5)$$

$$C_3 \geq 2C_2 \quad (6)$$

B. Tone-Decoder: Design and Experimentation

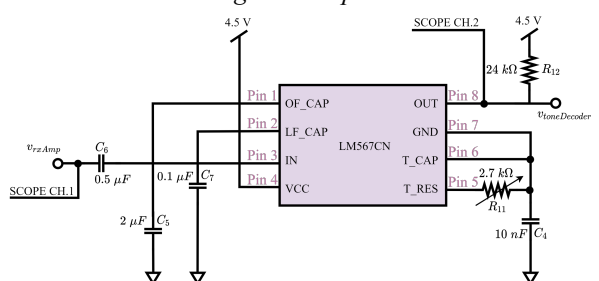


Fig. 19. The experimental setup to test the PLL-based 40kHz tone decoder built around the LM567CN.

According to (4), the following components, shown in Fig. 19, established a 40kHz center frequency within the tone decoder: $R_{11} = 2.7k\Omega$ and $C_4 = 10nF$. Assuming the input voltage is likely above 200mV, $C_7 = 0.1\mu F$ set a 3.2kHz detection bandwidth, 8% of the center frequency [5]. Lastly, $C_5 = 2\mu F$ to satisfy (6). Verifying proper operation of this circuit required powering the circuit and ensuring a 40kHz semi-triangular oscillation existed on pin 6 of the LM567CN. This free-running frequency was measured to be exactly 40.11kHz. To test it, the previously designed one-shot sent a 40kHz burst to the Tx driver which the Tx transducer emitted. The Rx transducer then received the reflected signal, a wavelet, which the Rx amplifier applied a gain to and inputted to the tone decoder. Fig. 20 shows the tone decoder locking on to that 40kHz wavelet.

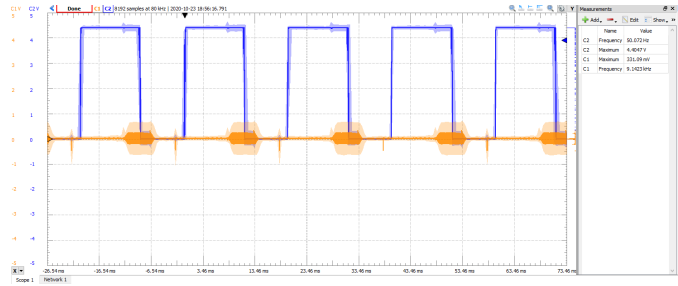


Fig. 20. An AD2 oscilloscope image showing the output of the wavelet output of the Rx amplifier on Ch.1 (orange) and output of the tone decoder on Ch.2 (blue). The ultrasonic transducer pair was 3m away from a wall for this test.

It was also desirable to measure the locked and capture range of the tone decoder. To do this, the AWG directly inputted into the tone decoder a 700mV sine wave whose frequency was varied. Measuring the locked range required starting the system in the locked condition ($V_{toneDecoder} = 0V$) and varying the input signal frequency up and down to see where the output goes to 4.5V. This measurement yielded a locked range from 36.1kHz to 41.6kHz, for a total range of 5.5kHz. Measuring the capture range required starting the system in the unlocked condition ($V_{toneDecoder} = 4.5V$) and varying the input signal frequency up and down to see where the output goes to 0V. This measurement yielded a capture range from 38.4kHz to 41.0kHz, for a total range of 2.6kHz.

VII. CRYSTAL OSCILLATOR

A. Crystal Oscillator: Theory

An oscillating circuit generated the 40kHz burst instead of the AD2. For this device, a Pierce crystal oscillator sufficed. In its simplest form, shown in Fig. 21, an oscillator is a filter and inverting amplifier operating on a positive feedback loop. For sustained oscillation, this circuit must satisfy the Barkhausen criteria in that it must have 0° phase shift and a loop gain greater than unity (0 dB) at the resonant frequency [8]. The amplifier and filter each impose a 180° for an overall phase shift of 360° or 0° .

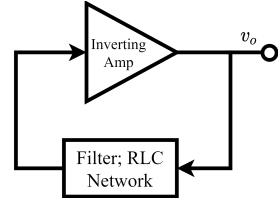


Fig. 21. A high-level block diagram of an oscillator.

While it is possible to build the filter out of resistors, inductors, and capacitors, those components are subject to frequency variations due to temperature, power-supply voltage, and mechanical vibrations [8]. A better alternative is to use quartz crystals which have stable, mechanically tuned natural oscillation frequencies. These are high-quality factor (Q) devices meaning they have a very narrow bandwidth, a desirable trait for a circuit expected to have a single sustained frequency. Unfortunately, the high Q characteristic makes it difficult to simulate in a program like LTSpice. Fig. 22 shows an RLC-based model of a crystal. C_1 is the motional arm capacitance (typically in the fF range), L_1 is the motional arm inductance (typically in the mH range), R_1 represents the resistive losses of the crystal (typically in the sub $k\Omega$ range), and C_0 is the shunt capacitance (typically in the pF range) [8]. Based on this model, the crystal has a series and parallel frequency, given by (7) and (8), which tightly surround its natural frequency $f_{crystal}$. Below f_{series} and above $f_{parallel}$, it acts capacitively [8]. In between, it acts inductively. Thus, assuming (9) holds, a load capacitance C_L in parallel with the crystal to cancel out that inductive reactance allows it to oscillate at $f_{crystal}$.

$$f_{series} = \frac{1}{2\pi\sqrt{L_1 C_1}} \quad (7)$$

$$f_{parallel} = \frac{1}{2\pi\sqrt{L_1 \frac{C_1 C_0}{C_1 + C_0}}} \quad (8)$$

$$f_{series} < f_{crystal} < f_{parallel} \quad (9)$$

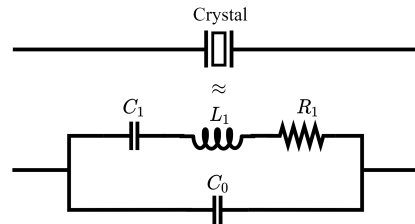


Fig. 22. The simplified electrical model of a quartz crystal [8].

B. Crystal Oscillator: Design and Experimentation

Fig. 23a shows the experimental design of a Pierce crystal oscillator for the range finder. It featured a CD4069UBE inverter and an ECS-.400-12.5-13X 40kHz quartz crystal. The designer must choose C_8 and C_9 for C_L specified in the crystal's datasheet [2]. Ideally, $C_8 = C_9 = C_L$, but along with parasitic capacitances, while the circuit is active, the inverter has an input capacitance specified as 10-15pF from its datasheet [9]. Fig.

23b shows the oscillator output after it reached steady-state operation.

$$\begin{aligned}
 C_8 &\approx 2C_L - C_{in,inverter} - C_{parasitics} \\
 C_8 &\approx 2(12.5pF) - 15pF - C_{parasitics} \\
 C_9 &\approx 2C_L - C_{parasitics} \\
 C_9 &\approx 2(12.5pF) - C_{parasitics} \\
 \Rightarrow C_8 &= 15pF, C_9 = 18pF
 \end{aligned}$$

It was important to use an unbuffered inverter to avoid any propagation delay that may keep the system from oscillating correctly. The bias resistance R_{bias} is there to bias the inverter at half the supply (0V) such that it operates as an amplifier with 10-20V/V gain. The large size of R_{bias} ensures that, after the Miller effect reduces its effective size by that 10-20V/V gain factor, the effective input resistance of the amplifier is still large enough that it does not load the preceding circuit and prevent oscillations.

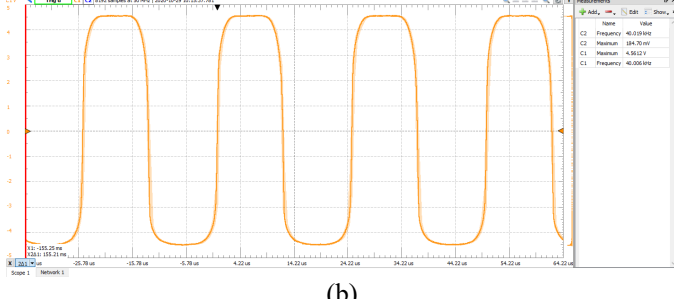
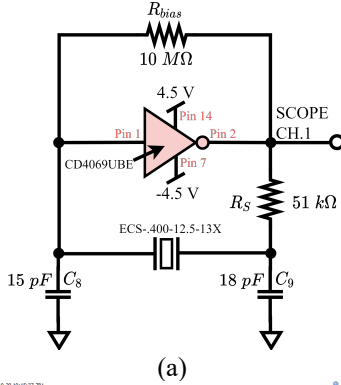


Fig. 23. (a) The experimental setup of the Pierce oscillator using the ECS-400-12.5-13X 40kHz crystal and the CD4069UBE hex inverter. (b) The Pierce oscillator output with an output buffer (another CD4069UBE inverter).

Before inserting the oscillator into the circuit, it is possible, via open-loop tests on the configuration shown in Fig. 24, to verify that it will oscillate. While the AD2 has a network analyzer to obtain frequency responses, it does not perform well with high Q circuits like this. So instead, the AWG inputted a 200mV sinusoidal signal. The oscilloscope's Ch.1 measured the input of the circuit and Ch.2 measured the output. The first thing to verify was zero phase shift between the input and output signal. The second thing to verify was more than unity gain at the resonant frequency of 40kHz.

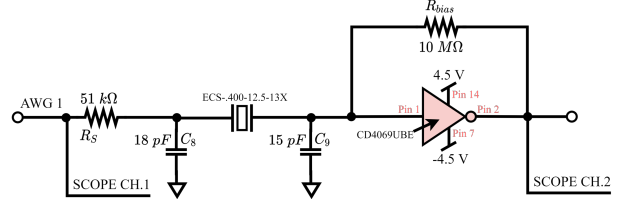


Fig. 24. The open-loop experimental circuit of the Pierce oscillator.

Since this is a high Q circuit, tiny deviations from 40kHz resulted in poor gain, as shown in Fig. 25. From Fig. 26a, the circuit had greater than unity gain and zero phase shift with the input signal at 40kHz. However, at 40.01kHz, in Fig. 25b, the gain dropped below unity.

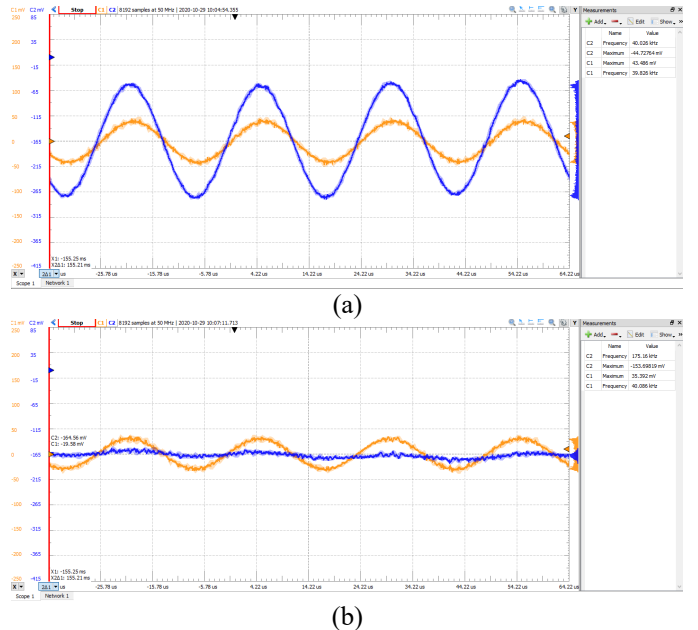
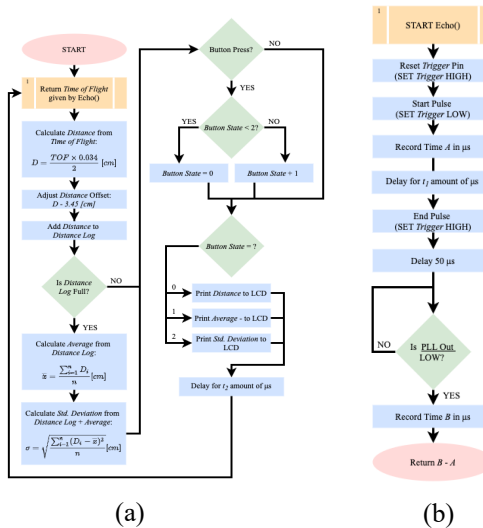


Fig. 25. (a) The input on Ch.1 (orange) and the output on Ch.2 (blue) of the open-loop test for the Pierce oscillator at 40kHz. (b) The same test but with a 40.01kHz signal.

VIII. MICROCONTROLLER

A. MicroController: Design and Experimentation

The microcontroller interfaced with both the user and analog circuitry. Moreover, the microcontroller also processed distances, from which it calculated the mean and standard deviation. The process flow diagrams of both the program and echo subroutine are shown in Fig. 26a and b. From Fig. 26a, the program has three areas of operation: range detection, distance calculation, and user interface. These areas occur sequentially, as listed previously.



(a)

(b)

Fig. 26. (a) The overhead process flow diagram of the program executed by the microcontroller. (b) The process flow diagram of the echo subroutine that the microcontroller used to interface with the analog circuitry and determine the time of flight.

At the start of the program, the microcontroller enters the Echo() subroutine where it interfaces with the analog circuitry. Referencing the flow diagram in Fig. 26b, the microcontroller pulsed the trigger pin per predefined amount of time, t_1 . For the final design, t_1 is 10 microseconds, sufficient enough to trigger the one-shot. During the low pulse, the program stores the time which it later references for calculating the time of flight. Following the pulse sent by the microcontroller the subroutine delays for 50 microseconds, avoiding mistriggering on reflections and crosstalk—50 microseconds translates to detection at one centimeter. Once the delay has elapsed, the program begins to poll the PLL output for a low pulse. Given that the microcontroller detects a low pulse, it records the time of detection, and the subroutine then returns the difference between the second and first recorded times.

Post determining the time of flight, the program goes on to calculate the distance. After testing the system several times, the measured distances suggested that the time of flight had a fixed offset. There may be several origins of the offset, chiefly in the use of delays during the Echo() subroutine. Tuning the duration and placement of the delays may mitigate the offset. However, the use of the offset adjustment seems to be adequate in garnering accurate measurements. The program used a rolling average for the average and standard deviation. The use of a rolling average allows for reduced latency and increased accuracy of measurements. The only downside is that it requires a 0.5-millisecond “start-up” period for the distance log to fill up.

Finally, after calculating the distance, average, and standard deviation, the program begins to check for user input. The only input given to the user is a button, which controls the metric printed to the LCD.

IX. POWER MANAGEMENT

A. Power Management: Theory

Since one of the goals of this project is to make the range finder portable, a battery provided the power supply, replacing the AD2. Given the current and voltage demands of the circuit, a 9V alkaline battery was an adequate supply. Moreover, the increased voltage level means an increased wavelet amplitude both before and after amplification. This increase in signal strength should allow for improved distance measurements by increasing the detection range. Since several of the subcircuits operate at a max supply voltage of 5V, the system must regulate the 9V battery down to 5V. Fig. 27 shows the optimal voltage divider for a 5V output from the voltage regulator.

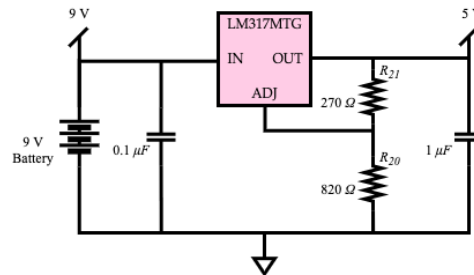


Fig. 27. Linear voltage regulator circuit that supplied both the 5V and 9V rails

The advantage of using a separate 5V rail other than the one provided by the microcontroller was due to the current needed. If the 5V pin on the microcontroller powered the system, the microcontroller would not be able to supply adequate current to power the system in its entirety.

B. Power Management: Design and Experimentation

Due to the integration of the battery, the system had three distinct rails: 0V, 5V, 9V. The variety in voltages is well suited in optimizing the performance of the circuit while maintaining the functionality. The subcircuits supplied between 0V-5V were the one-shot, the gating circuit, and the tone decoder. The subcircuits supplied between 0V-9V included the Tx driver, crystal oscillator, and Rx amplifier(s). Moreover, the input to the Rx amplifier(s) stayed at 4.5V to ensure that the incoming wavelet would be able to saturate the amplifier and use the full range from 0V to 9V on the output.

X. DESIGN IMPROVEMENTS

A. Design Improvements: Theory

While and after testing, the system’s performance suggested that accurate distance measurements relied on the tone decoder’s consistency. Thus, changes to that circuit, although small, resulted in immense impacts on the system’s performance. The first change was to the output of the tone decoder. To reduce the triggering of the tone decoder, a capacitor shunted the output to ground. Another change was to the input capacitor of the tone decoder, going from $0.5\mu\text{F}$ to $1\mu\text{F}$. The increased size of the AC coupling capacitor helped

trigger the tone decoder more consistently. These changes are shown below in Fig. 28.

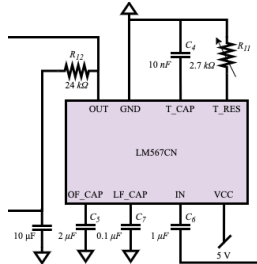


Fig. 28. Changes made to tone decoder to improve input and output signal quality

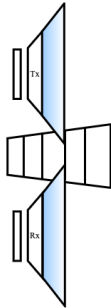


Fig. 29. Changes made to the transducers to improve signal quality

Another change made to the system was the cones on each transducer along with a piece of porous and reflective material in between, as Fig. 29 shows. The cones directed the signal while the divider material helped diminish the crosstalk between both transducers. As a divider material, foil and foam dampened stray sound waves.

Finally, the last modification made to the system was in changing the BJT op-amp IC for the CMOS op-amp IC. By using the CMOS op-amp, the amplification of the incoming wavelet. Since the CMOS chip lacks a gate current, the input impedance is much greater than that of the BJT chip. Moreover, the voltage-controlled nature of the CMOS op-amp is more reliable in amplifying the wavelet than the current controlled nature of the BJT chip. This reliability appears because the transducers don't source current but rather create a voltage differential when excited (i.e. vibrated).

B. Design Improvements: Design and Experimentation

As mentioned previously, upon testing the circuit, an offset to the distance measurements appeared. Moreover, the variance of the measured distance given across any short interval of time shows noise present in the recorded distances. Since the noise followed linearly with the range measurements, the program could average out the noise to acquire a reliable reading. The offset adjustment and rolling average comprised the real-time post-processing used to display a semi-accurate measurement. Fig. 30 plots the pre/post-processed results and the actual distance versus time.

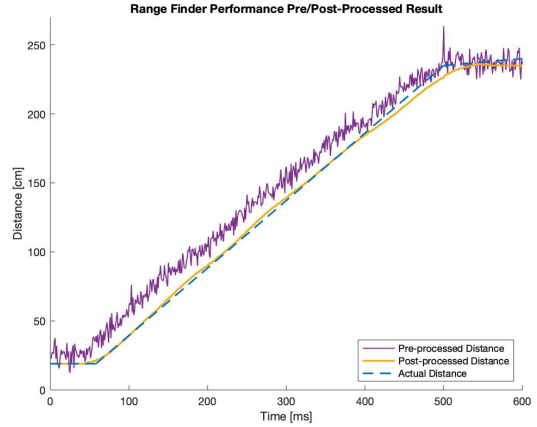


Fig. 30. The microcontroller connection scheme to analog circuitry and user interface (LCD, button)

As shown in Fig. 30, the post-processed distances were fairly close to the actual distances. This only remained true for distances in the range of 6 to 250 centimeters. Distances closer or further away were unreliable. The failure to detect at further than 2.5 meters may have been due to the poor acoustics in the environment. Sound dampening material enclosing the range finder may reduce multipathing. As for distances closer than 6 centimeters, better shielding between the two transducers may be able to decrease the crosstalk, which allows for the system to properly trigger on the desired wavelet. The final circuit is shown below in Fig. 31.

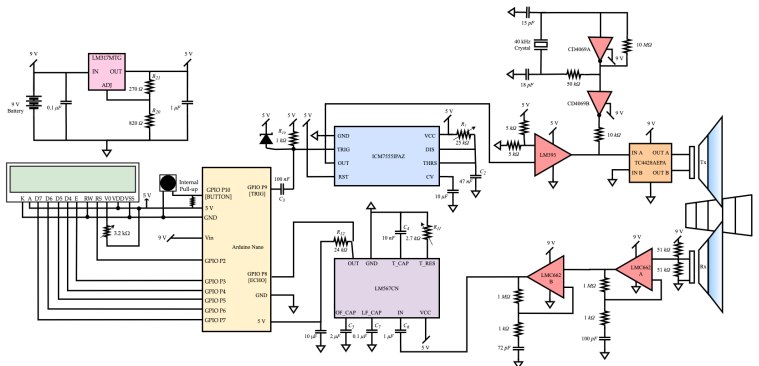


Fig. 31. Complete system circuit diagram with subsystem modifications

REFERENCES

- [1] V. Prodanov, "Modified EE449 for Remote Delivery (Fall 2020)", California Polytechnic State University EE 449 Laboratory Manual, July, 2020.
 - [2] ECS Inc. International, "The ECS-31X Series low frequency tuning fork crystals offer low frequencies in a compact thru hole package", ECS Inc. International, 2017. [Online] Available: <https://www.mouser.com/datasheet/2/122/ecs-31x-669.pdf>
 - [3] Microchip, "1.5A Dual High-Speed Power MOSFET Drivers". Microchip Technology, 2004. [Online] Available: <https://www.mouser.com/datasheet/2/268/2142c-73495.pdf>
 - [4] Texas Instruments, "LM158, LM158A, LM258, LM258A LM358, LM358A, LM358B, LM358BA, LM2904, LM2904B, LM2904BA, LM2904V SLOS068X Industry-Standard Dual Operational Amplifiers", Texas Instruments, June, 2020. [Online] Available: <https://www.ti.com/lit/ds/symlink/lm358.pdf?HQS=TI-null-null->

- [mousermode-df-pf-null-wwe&ts=1600309971992&ref_url=https%253A%252F%252Fwww.mouser.com%252F](https://www.mouser.com/df-pf-null-wwe&ts=1600309971992&ref_url=https%253A%252F%252Fwww.mouser.com%252F)
- [5] Texas Instruments, “LM567x Tone Decoder”, Texas Instruments, December, 2014. [Online] Available: https://www.ti.com/lit/ds/symlink/lm567c.pdf?HQS=TI-null-null-mousermode-df-pf-null-wwe&ts=1600310192905&ref_url=https%253A%252F%252Fwww.mouser.com%252F
- [6] Renesas, “ICM7555, ICM7556 General Purpose Timers”, Renesas, March, 2020. [Online] Available: <https://www.mouser.com/datasheet/2/698/icm7555-56-1528913.pdf>
- [7] Texas Instruments, “LM393B, LM2903B, LM193, LM293, LM393 and LM2903 Dual Comparators”, Texas Instruments, October, 2020. [Online] Available: https://www.ti.com/lit/ds/symlink/lmc662.pdf?HQS=TI-null-null-mousermode-df-pf-null-wwe&ts=1600309904367&ref_url=https%253A%252F%252Fwww.mouser.com%252F
- [8] S. Bible, “Crystal Oscillator Basics and Crystal Selection for rfPICTM and PICmicro® Devices”, Microchip Technology Inc., 2002. Available: <http://ww1.microchip.com/downloads/en/AppNotes/00826a.pdf>
- [9] Texas Instruments, “CD4069UB CMOS hex inverter”, Texas Instruments, January, 2019. [Online] Available: https://www.ti.com/lit/ds/symlink/cd4069ub.pdf?HQS=TI-null-null-mousermode-df-pf-null-wwe&ts=1600309904367&ref_url=https%253A%252F%252Fwww.mouser.com%252F
- [10] Arduino, “Arduino Nano: Technical Specs”, Arduino.cc, 2020, Available: <https://www.arduino.cc/en/pmwiki.php?n>Main/ArduinoBoardNano>